PAPER

Check for updates

Self-assembled rosette nanotubes from tetra guanine-cytosine modules†

Usha D. Hemraz, [ID] *[abc] Takeshi Yamazaki,[ab] Mounir El-Bakkari,[ab] Jae-Young Cho[b] and Hicham Fenniri*[abd]

Self-assembly of small molecules into supramolecular architectures is a sustainable alternative to new advanced material design. Herein, the design and synthesis of a self-assembling system containing four covalently linked hybrid guanine and cytosine (G∧C) units that were connected through bifunctional amines are reported. These tetra G∧C motifs were characterized and self-assembled in water and methanol to produce discrete nanostructures. Each module has 24 sites for intermolecular hydrogen bonding and it is proposed that in solution the four G∧C units per molecule align into a linear stack which in turn self-assembles into a hexameric super-helix held together by 72 intermolecular hydrogen bonds. Stacking of these nano-helices led to the formation of quad rosette nanotubes.

Introduction

Nature relies on a number of large and complex architectures to perform sophisticated processes, which demand the co-ordination of both non-directional and directional non-covalent interactions.[1–3] Achieving the level of complexity and molecular recognition ability as natural systems entail in-depth understanding of the forces and interactions that propel such organization. Still, a variety of artificial self-assembled structures have emerged.[4–10] The majority of self-assembled supra-molecular systems have been based on the built-in hydrogen bonding complementarity and directionality of the monomers, hydrophobic effects and aromatic stacking interactions.[11–16]

Among such self-assembled systems, rosette nanotubes (RNTs) are biologically inspired nanomaterials, formed from the hierarchical self-assembly of a hybrid guanine-cytosine motif (G∧C) featuring self-complementary hydrogen-bonding arrays.[17–20] In solution, the G∧C base forms six-membered rosettes, which then stack into a tubular architecture. The length and the diameter of RNTs can be readily tuned[21–23] and their applications in tissue engineering,[24–30] cargo delivery,[31–33] simulation[34,35] and material science,[36–38] was made possible due

[a]Department of Chemistry, University of Alberta, 11227 Saskatchewan Drive, Edmonton, Alberta, T6G 2G2, Canada

[b]Nanotechnology Research Centre, National Research Council of Canada, 11421 Saskatchewan Drive, Edmonton, Alberta, T6G 2M9, Canada. E-mail: Usha.Hemraz@nrc-cnrc.gc.ca

[c]Human Health Therapeutics, National Research Council Canada, 6100 Royalmount Avenue, Montreal, Quebec, H4P 2R2, Canada

[d]University Mohammed VI Polytechnic, Lot 660, Hay Moulay Rachid, 43150 Benguerir, Morocco. E-mail: hicham.fenniri@um6p.ma

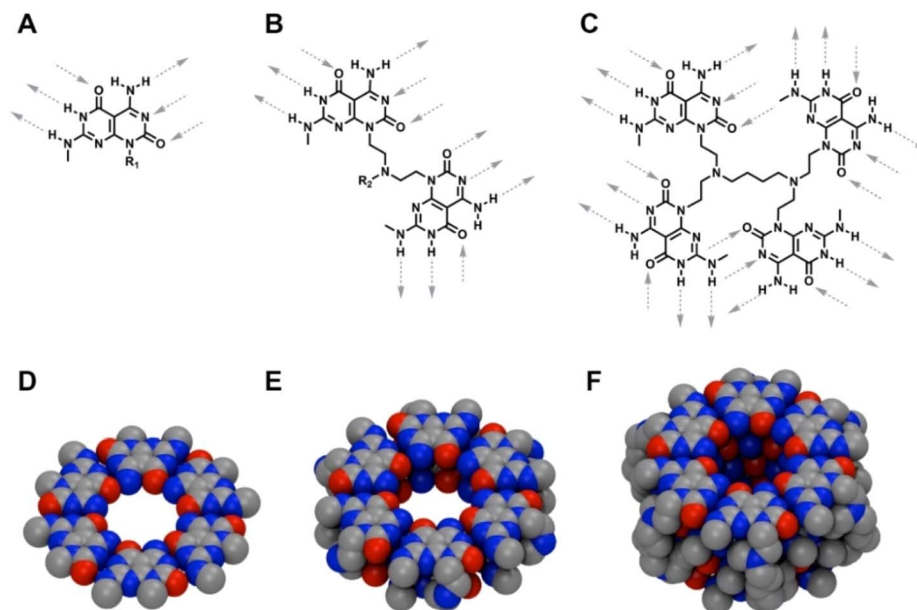† Electronic supplementary information (ESI) available. See DOI: https://doi.org/10.1039/d4na00567h

to their synthetic accessibility and chemical tunability. Our group has worked on the design of two main families of RNTs: (1) a single G∧C base with six sites for intermolecular hydrogen bonding in a spatial arrangement that forces the modules to form a hexameric super-macrocycle, which are maintained by 18 H-bonds (Fig. 1A),[16,17] and (2) two covalently-linked G∧C bases in a stacked *syn* arrangement that led into a six membered twin rosette system maintained by 36 H-bonds (Fig. 1B).[22] Though both the single and twin G∧C systems have built-in ability to engage in intermolecular hydrogen-bonding, the twin G∧C variant is more stable and yield RNTs at a faster rate due to lower functional group density, reduced net charge, enhanced stability arising from preorganization, increased amphiphilic character, greater number of H-bonds per module, higher number of H-bonds per rosette (36 H-bonds instead of 18), less steric congestion and lower electrostatic repulsion.[22] The design of the twin RNTs is so robust that it can withstand higher temperatures, broad pH range, and sterically demanding functional groups.[23,25,26,39] To test the limits of this design, we synthesized a library of peptide-functionalized RNTs varying in length from 1 to 15 lysine residues, and investigated their self-assembling properties.[23,33] While these modules formed RNTs, a decrease in stability was noted as the peptide moiety was lengthened. The modules bearing peptides of 10 or more amino acids required alkaline conditions to reduce the electrostatic repulsion and form RNTs. This observation prompted a quest to design a self-assembling core containing more than two G∧C units. We presumed that they would in turn be maintained by a higher number of intermolecular hydrogen bonds than the 36 H-bonds for the twin G∧C system. The new system could potentially withstand a higher steric bulk and self-assemble at physiological conditions for any prospective biological appli-cations. Herein, we report the design and synthesis of a self-

Fig. 1 Structures of: single G∧C rosette with 3 donor and 3 acceptor sites for hydrogen bonding (A); twin G∧C rosette with 6 donor and 6 acceptor sites for hydrogen bonding (B) and tetra G∧C rosette with 12 donor and 12 acceptor sites for hydrogen bonding (C). Top view of: single G∧C rosette (D), twin G∧C rosette (E) and tetra G∧C rosette (F), held by 18, 36 and 72 hydrogen bonds, respectively and obtained through simulation.

assembling system containing four covalently linked G∧C moieties that were connected using bifunctional amines. The presence of ample hydrogen bonding sites led to the self-assembly of the newly synthesized tetra G∧C molecules to produce nanotubes. This new self-assembling tetra G∧C system could be useful in the design of nanomaterials that could sustain higher steric bulk.

Results and discussion

The tetra-G∧C module **4a** was synthesized in two steps starting from G∧C aldehyde **2** (Scheme 1). The latter, which was synthesized starting from barbituric acid accordingly to a previously reported procedure,[19,20] was coupled with the commercially available 1,4 diaminobutane **1a** through a reductive amination reaction to yield the benzyl and Boc-protected tetra-G∧C **3a**. Removal of the protecting groups under acidic conditions afforded **4a** as a hydrochloride salt in quantitative yield. A similar procedure was applied for the synthesis of monomers **4b** and **4c** using oligoethyleneoxide diamines **1b** and **1c**, respectively. Unlike the tetra-G∧C module **4a** where the linker consisted of a four-carbon aliphatic chain, the tetra-G∧C modules **4b** and **4c** were made of ether linkages of varied length.

By design, the G∧C motif has built-in hydrogen bonding sites that allows the system to self-assemble. We have previously shown the design and self-assembly of the single and twin G∧C building blocks. Unlike the single (Fig. 1A) and twin (Fig. 1B) G∧C motifs that have six and twelve sites available for intermolecular hydrogen bonding per molecule, the newly synthesized tetra-G∧C module possesses twenty-four intermolecular hydrogen-bonding sites (Fig. 1C). To maximize the use of all

twenty-four intermolecular hydrogen-bonding sites per module, the tetra-G∧C building blocks could self-organize into linear stacks, which would in turn self-assemble into a hexameric super-helix held together by 72 intermolecular hydrogen bonds (Fig. 1F).

Next, the self-assembly of tetra-G∧C modules were investigated. The self-assembly of **4a** was carried out in methanol and water, whereby discrete structures were observed in both solvents (Fig. 2A and B). The nanostructures seemed to form larger aggregates in water (Fig. 2B, S1 and S3†) compared to methanol (Fig. 2A and S2†). Since the SEM images of **4a** in water showed a larger diameter than what is usually observed for a RNT, RNTs self-assembled from **4a** and a twin G∧C module (But-TBL, Scheme 1) separately were imaged on the same TEM grid (Fig. 2C) to have a better visual comparison of dimensions. The twin G∧C module But-TBL self-assembles into a hexameric macrocycle held together by 36 hydrogen bonds, with a theoretical diameter of 3.4 nm.[31] The electron microscopy data displayed nanostructures of two distinct dimensions that were obtained through measurements, with a larger diameter of 7.3 ± 0.3 nm corresponding to **4a** and a smaller diameter of 3.3 ± 0.2 nm resulting from But-TBL.[25,31] However, a careful analysis of the TEM images revealed that the larger nanostructures were in fact made up of two or three thinner tube-like structures (Fig. 2D and S3†), with an average diameter of a single tube of 3.2 ± 0.1 nm in both solvents. The same difference in the theoretical diameters of the hexameric macrocycles from **4a** (3.1 nm) and But-TBL (3.4 nm) is attributed to the butyl ammonium side chain in the latter.

The simplest way that the tetra-G∧C system **4a** could yield a diameter of about 3.2 nm was to mimic the self-assembly of
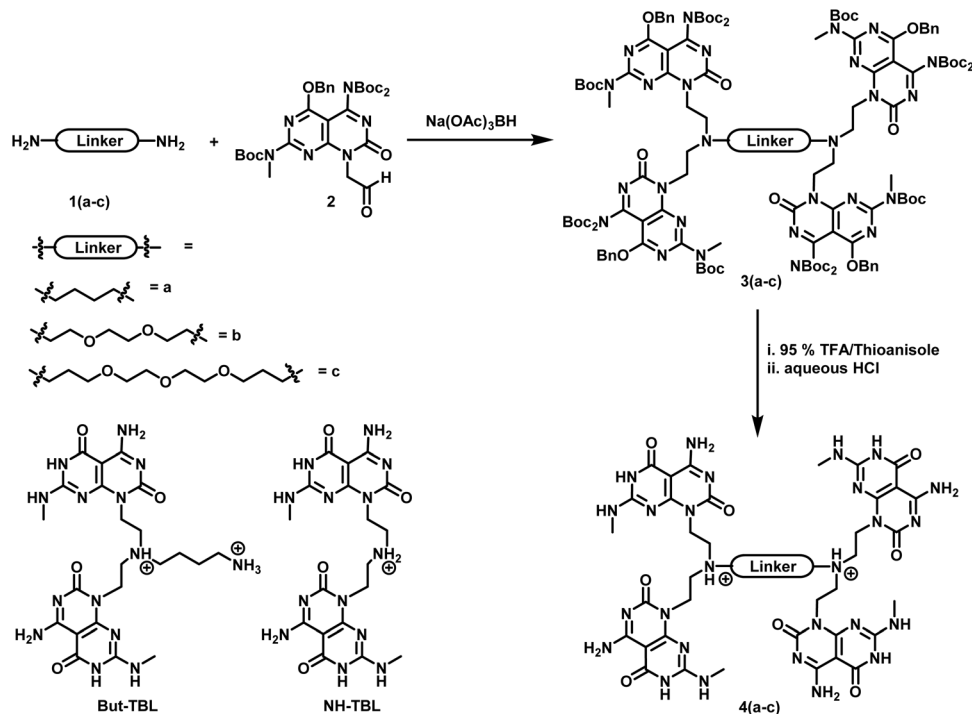
Scheme 1 Synthetic route for the formation of tetra G∧C modules **4(a–c)** and structures of twin G∧C modules But-TBL and NH-TBL.
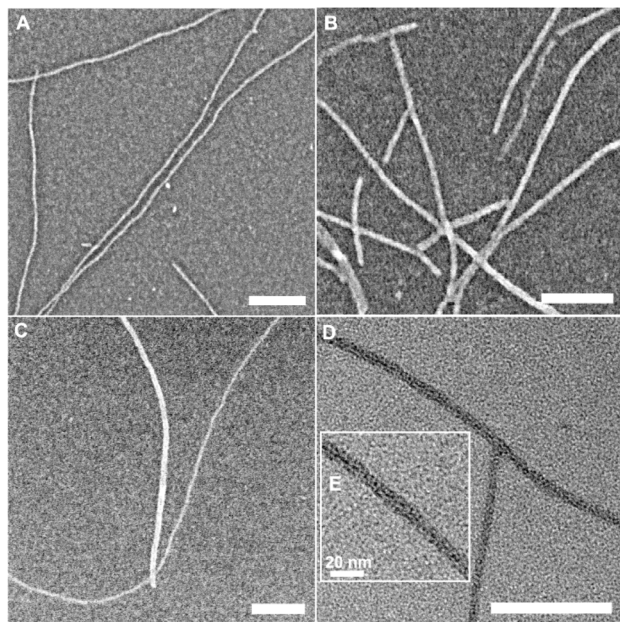

Fig. 2 SEM images of **4a** module in methanol (A), in water (B), co-deposited with But-TBL in water (C), TEM image of **4a** in water (D), and an inset to show individual RNTs (E). Scale bar = 100 nm.

the twin G∧C system. As mentioned earlier, self-assembly in a twin G∧C system involves the *syn* intramolecular stacking of the two G∧C units, followed by the formation of a six membered macrocycle held by 36 H-bonds. The four G∧C units in module **4a** can be considered as a pair of twin G∧C stacks tethered by

a linker. Due to the favourable π–π interactions between the G∧C units and intramolecular hydrogen bonding of the ammonium ion and carbonyl oxygen of the cytosine ring, we presumed that the four G∧C units could stack into a 4-fold pile. This hypothesis was verified computationally (Fig. 3). Starting from a quad-rosette ring consisting of six motifs with a *syn–syn–syn* conformation (SSS) (Fig. 3B), the geometry of the ring was optimized, following previous modeling studies for single and twin G∧C systems. Upon optimization, it was found that the G∧C units aligned themselves in a displaced stacking fashion, with a zig-zag type arrangement of the methyl groups (Fig. 3C and D). This could have been triggered by the relatively short length of the linker in **4a** that could exert a certain degree of strain on this strand due to the limited flexibility of the tether. We believe that alignment in a displaced fashion could allow the G∧C units to offset this strain. The outer diameter of this quad-rosette was calculated to be 3.1 nm. With this arrangement, there was an optimal use of the hydrogen-bond donor and acceptor sites, where each molecule was involved in 24 H-bonds, and a total of 72 intermolecular H-bonds per quad-rosette. A similar quad-rosette ring was constructed with a *syn–anti–syn* (SAS) arrangement of the G∧C moieties to give a rosette ring with an outer diameter of 3.1 nm (Fig. 3E and F).

Experimentally, the tetra-G∧C module **4a** could form nanotubes (Fig. 2) and the quad-rosettes from **4a** of SSS and SAS configurations produced nanotubes with a calculated outer diameter of 3.1 nm (Fig. 4A, B, respectively and S6†). Next, the relative stabilities of the resulting nanotubes were calculated and compared to the twin RNT NH-TBL (resulting from coupling of ammonia with two molecules of a G∧C derivative,
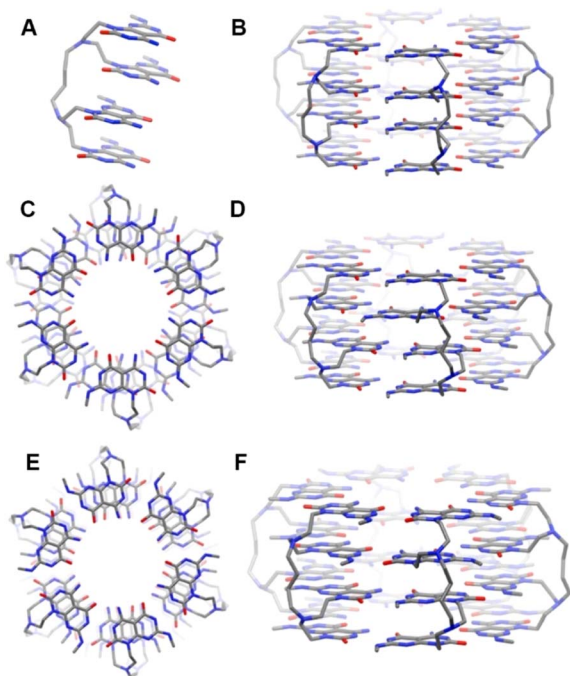
Fig. 3 Side view of an all-*syn* quad-rosette from the **4a** monomer (A) and side view of the unoptimized quad-rosette ring (B); top view (C) and side view (D) of the optimized quad-rosette ring with a SSS conformation, showing displaced stacks of G∧C units; and top view (E) and side view (F) of the optimized quad-rosette ring from **4a** with a SAS conformation and displaced stacks of G∧C units.
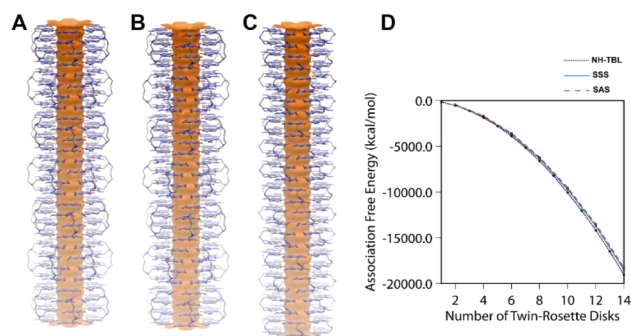

Fig. 4 Nanotubes made up of 7 quad-rosettes from **4a** with SSS (A) and SAS (B) arrangements of the G∧C units, and nanotube derived from NH-TBL (C), generated by the stacking of 14 twin-rosettes through simulation. Comparison of association free energies of nanotubes from **4a** with SSS and SAS arrangements of the G∧C units with increasing number of rosette stacks (up to 7 stacks), and of NH-TBL (up to 14 stacks) (D).

Scheme 1). To justify for the difference in the number of the G∧C units, each quad-rosette ring from **4a** was accounted for two twin rosette rings. From the association free energy plot, it was found that NH-TBL and the two possible conformers of the **4a** module had comparable stabilities (Fig. 4D). Although in this work a comparison of a twin-G∧C containing a bulky side chain was not carried out against the tetra-G∧C module with a similar pendant, it is speculated that the tetra-G∧C would have a higher

stability when carrying an analogous bulk as compared to twin-G∧C due to the increase in the number of hydrogen bonding per rosette. Despite the limited flexibility of the hydrophobic butyl linker in the strand, negative association free energies of the SSS and SAS nanotubes in water suggested that the solvent plays an important role in the formation of such superstructures. The solvophobicity of the **4a** module in water is greater than that in methanol. As such, the higher solvophobic interactions in water leads to the formation of RNTs' aggregates, which could explain the formation of RNTs' bundles in water and the isolated RNT in methanol.

Apart from the SSS and SAS conformations for **4a** using molecular modelling, two other supramolecular structures were explored (Fig. S7†). Firstly, a six-membered ring structure with a 5.1 nm diameter was studied, whereby only two of the four G∧C units were involved in intermolecular hydrogen bonding (Fig. S8†). While this arrangement did mimic the twin-RNT system, the free hydrogen-bond donor and acceptor sites of the two remaining G∧C units were free to engage in intermolecular interactions. In the second case, a four-membered ring structure with an outer diameter of 3.6 nm was obtained (Fig. S9†). Both conformations were unlikely since they cannot produce discrete architectures and do not have the correct geometry for hydrogen bonding and intermolecular π–π stacking of the G∧C units.

The module **4a** self-assembled readily in water. However, given that built-in linker was hydrophobic, aggregation was observed in water. For any prospective biological applications, we believe that it is important for the monomers to self-assemble into well-dispersed nanostructures under physiological conditions. Therefore, analogues (**4b** and **4c**) of the **4a** motif were designed to test the effect of longer and more hydrophilic linkers on self-assembly and whether the aggregation observed was only a consequence of the hydrophobic nature of the linker. The ether linkages incorporated in the system design of **4b** and **4c** provided a boost in the hydrophilicity of the monomers. The presence of the oxygen atoms in the linker resulted into well-dispersed single tubes in water, as observed from the microscopy images (Fig. 5A, B, S4 and S5†). The measured diameters obtained by TEM were 3.4 ± 0.2 nm and 3.4 ± 0.1 nm respectively. This data was in agreement with TEM measurement observed for the **4a** building block and is therefore in line with
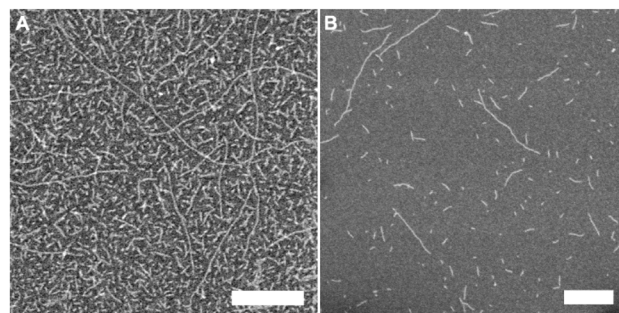

Fig. 5 SEM images of **4b** (A) and **4c** (B) modules in water. Scale bar = 100 nm.

the proposed formation mechanism of the self-assembled structures. The present observation also provides evidence that RNTs consisting of the **4a** motif form bundles based on the solvophobic (hydrophobic) interactions in water, where the tetra-G∧C system had preferential parallel formation of nanotubes.

Experimental section

General methods

Unless stated otherwise, all reactions were performed under N_2 atmosphere. Reagent grade solvents (DCM, 1,2 DCE) were purified using the solvent purification system and all other commercial reagents and solvents were used as purchased. The G∧C aldehyde 2 was synthesized according to a previously reported procedure. Reactions were monitored by TLC using silica-coated TLC plated and were visualized under UV light. The NMR data is presented as follows: chemical shift, multiplicity, coupling constant, integration. The following abbreviations were used for the multiplicities: s = singlet, d = doublet, t = triplet m = multiplet, bs = broad singlet. Residual ^1H shifts in $CDCl_3$ (7.24 ppm), d_1-TFA (11.50 ppm), d_6-DMSO (2.50 ppm) and CD_2Cl_2 (5.30 ppm) were used as internal references. Similarly, $CDCl_3$ (77.23 ppm), d_1-TFA (164.2 ppm), d_6-DMSO (39.51 ppm) and CD_2Cl_2 (53.8 ppm) were used as internal references for ^{13}C NMR. The ^1H NMR and ^{13}C NMR spectra were calibrated using 3-(trimethylsilyl)-1-propanesulfonic acid sodium salt (TMS = 0.0) as the internal reference.

Synthetic procedures

Synthesis of compound 3a (Scheme 1). 1,4-Diaminobutane (0.015 g, 0.170 mmol) was added to a stirred solution of compound **2** (0.200 g, 0.313 mmol) in 1,2 dichloroethane (DCE) (20 mL) at room temperature under N_2. The solution was stirred for 30 min before adding sodium triacetoxy borohydride (0.070 g, 0.333 mmol) and stirring was maintained for an additional 24 h. The reaction mixture was diluted with CH_2Cl_2 (50 mL) and then washed with water (10 mL), $NaHCO_3$ (10 mL), brine (15 mL), dried over Na_2SO_4 and concentrated. Fresh 1,2 DCE (20 mL) and compound **2** (0.200 g, 0.313 mmol) were then added to the pale-yellow foam and stirred. Sodium triacetoxy borohydride (0.075 g, 0.357 mmol) was then added in aliquots (0.025 g each) at 0.5 h, 4 h and 24 h. The resulting solution was stirred for another 24 h. The reaction mixture was diluted with dichloromethane (DCM) (50 mL) and then washed with water (10 mL), $NaHCO_3$ (10 mL), brine (15 mL), dried over Na_2SO_4 and concentrated. Flash chromatography of the residue over silica gel (0–70% EtOAc in hexanes) gave **3a** as a white foam in 62% yield. R_f = 0.53 (70% EtOAc in hexanes); ^1H NMR (500 MHz, $CDCl_3$) δ 7.46–7.29 (m, 20H), 5.57 (s, 8H), 4.38 (t, J = 7.5 Hz, 8H), 3.50 (s, 12H), 2.88 (t, J = 7.5 Hz, 8H), 2.71 (bs, 4H), 1.55 (s, 36H), 1.48 (m, 4H), 1.30 (s, 72H); ^{13}C NMR (125 MHz, $CDCl_3$) δ 165.5, 161.2, 161.0, 155.5, 152.5, 149.1, 135.0, 128.6, 128.5, 128.5, 128.5, 127.9, 126.9, 92.8, 83.5, 82.8, 70.0, 65.3, 54.8, 51.0, 41.7, 35.0, 28.1, 27.8, 27.8, 25.3; HRMS (ESI+) calcd for $C_{128}H_{173}N_{26}O_{32}$ $[M + H]^+$ 2586.2704; found 2586.2716; anal.

calcd for $C_{128}H_{172}N_{26}O_{32}$ C, 59.43, H, 6.70, N, 14.08; found C, 59.62, H, 6.83, N, 13.14.

Synthesis of compound 4a (Scheme 1). Compound **3a** (0.123 g, 0.048 mmol) was stirred in a 95% TFA in thioanisole (10 mL) for 72 h. Diethyl ether (Et_2O) (60 mL) was then added to the reaction mixture and the precipitate formed was centrifuged down. The residual solid was resuspended in Et_2O, sonicated and centrifuged down. This process was repeated until spotting of the Et_2O produced no UV active spot. The white solid was dried under vacuum and then dissolved in 1 M hydrochloric acid (10 mL), followed by removal of water under reduced pressure. This process was repeated two more times to convert the TFA salt into the HCl salt. The solid was dried under vacuum for 72 h to yield the desired compound **4a** as an off-white powder ($C_{40}H_{52}N_{26}O_8$ + 8 HCl + $3H_2O$ + 0.5 Et_2O, 99%). ^1H NMR (600 MHz, d_6-DMSO) δ 12.26 (bs, 4H), 9.21 (s, 4H), 8.96 (s, 4H), 8.15 (s, 4H), 4.45 (s, 8H), 3.54 (s, 8H), 3.78 (s, 4H), 3.30 (s, 6H), 2.90 (d, J = 1.8 Hz, 12H), 1.80 (s, 4H); ^{13}C NMR (150 MHz, d_6-DMSO) δ 161.2, 160.3, 156.6, 156.2, 148.5, 83.1, 52.0, 49.6, 49.1, 36.7, 28.5; HRMS (ESI+) calcd for $C_{40}H_{53}N_{26}O_8$ $[M + H]^+$ 1025.4534; found 1025.4526. Anal. calcd for $C_{40}H_{52}N_{26}O_8$(HCl)$_8$(H_2O)$_3$ (Et_2O)$_{0.5}$ C, 35.83, H, 5.08, N, 25.87; found C, 35.32, H, 4.86, N, 25.99.

Synthesis of compound 3b (Scheme 1). 2,2′-(Ethylenedioxy) bis(ethylamine) (0.015 g, 0.1 mmol) and N,N'-diisopropylamine (DIEA) (0.11 mL, 0.61 mmol) were added to a stirred solution of aldehyde **2** (0.26 g, 0.4 mmol) in 1,2 DCE (5 mL) at room temperature under N_2. The solution was stirred for 30 min before adding sodium triacetoxy borohydride (0.1 g, 0.485 mmol). The resulting mixture was stirred for an additional 2 h, after which compound **2** (0.129 g, 0.2 mmol) was added to the reaction mixture, followed by addition of sodium triacetoxy borohydride (0.205 g, 0.97 mmol) in aliquots of 0.102 g at 5 min and 10 min. The resulting solution was stirred for another 2 h. The reaction mixture was diluted with DCM (50 mL) and then washed with water (20 mL), citric acid (30 mL), $NaHCO_3$ (30 mL), brine (20 mL), dried over Na_2SO_4 and concentrated. Flash chromatography of the residue over alumina gel (50–90% EtOAc in hexanes) gave **3b** as a pale-yellow oil in 78% yield.

^1H NMR (600 MHz, CD_2Cl_2) δ 7.46–7.30 (m, 20H), 5.57 (s, 8H), 4.35 (t, J = 7.2 Hz, 8H), 3.52–3.48 (m, 8H), 3.47 (s, 12H), 2.95–2.90 (m, 12H), 1.54 (s, 36H), 1.31 (s, 72H); ^{13}C NMR (150 MHz, CD_2Cl_2) δ 171.2, 166.1, 161.8, 161.6, 160.7, 155.9, 153.1, 149.8, 135.8, 129.0, 128.98, 128.95, 93.2, 83.9, 83.2, 70.8, 70.4, 70.3, 60.7, 54.1, 52.0, 41.9, 35.4, 28.4, 28.1; HRMS (ESI+) calcd for $(C_{130}H_{176}N_{26}Na_2O_{34})_{0.5}$ $[M/2 + Na]^+$ 1345.6313; found 1345.6306.

Synthesis of compound 4b. Compound **3b** (0.214 g, 0.081 mmol) was stirred in a solution of TFA (6 mL) and DCM (2 mL) for 72 h. Et_2O (60 mL) was then added to the reaction mixture and the white precipitate formed, was centrifuged down. The residual solid was resuspended in Et_2O, sonicated and centrifuged down. This process was repeated until spotting of the Et_2O produced no UV active spot. The white solid was dried under vacuum for 72 h to yield the desired compound **4b** as a white solid ($C_{42}H_{56}N_{26}O_{10}$ + 5.15 TFA + 0.25H_2O + Et_2O, 81%). ^1H NMR (600 MHz, d1-TFA) δ 4.76–4.66 (m, 8H), 4.01–3.77 (m,

Nanoscale Advances

20H), 3.13 (d, $J = 6.6$ Hz, 12H); ^{13}C NMR (150 MHz, D$_2$O/d1-TFA) δ 163.36, 161.47, 157.43, 157.19, 150.71, 83.89, 71.28, 65.09, 54.50, 53.45, 38.40, 28.74; MALDI-TOF MS (THAP, positive mode) calcd for C$_{42}$H$_{57}$N$_{26}$O$_{10}$ [M + H]$^+$ 1085.4745; found 1085.4741.

Anal. calcd for C$_{42}$H$_{56}$N$_{26}$O$_{10}$(CF$_3$CO$_2$H)$_{5.15}$(H$_2$O)$_{0.25}$(C$_4$H$_{10}$O), C, 38.62; H, 4.12; N, 20.80; found C, 38.85, H, 4.09, N, 20.67.

For the self-assembly study, an aliquot of the TFA salt of **4b** was converted to the HCl salt. Compound **4b** (TFA salt) (0.035 g, 0.020 mmol) was dissolved in 1 M hydrochloric acid (15 mL), followed by removal of water under reduced pressure. This process was repeated two more times before the solid was dried under vacuum for 72 h to give the HCl salt of **4b** as a white solid (C$_{42}$H$_{56}$N$_{26}$O$_{10}$ + 8 HCl + 2H$_2$O + 0.5 Et$_2$O, 87%). MALDI-TOF MS (THAP, positive mode) calcd for C$_{42}$H$_{57}$N$_{26}$O$_{10}$ [M + H]$^+$ 1085.4745; found 1085.4730; anal. calcd for C$_{42}$H$_{56}$N$_{26}$O$_{10}$(HCl)$_8$(H$_2$O)$_2$(C$_4$H$_{10}$O)$_{0.5}$, C, 36.45; H, 5.08; N, 25.12; found C, 36.44, H, 5.24, N, 24.91.

Synthesis of compound 3c. 4,7,10-Trioxa-1,13-tridecanediamine (0.015 g, 0.068 mmol) and DIEA (0.119 mL, 0.68 mmol) were added to a stirred solution of aldehyde **2** (0.218 g, 0.34 mmol) in 1,2 DCE (5 mL), at room temperature under N$_2$. The solution was stirred for 30 min before adding sodium triacetoxy borohydride (0.135 g, 0.64 mmol). The resulting mixture was stirred for an additional 20 h. Compound **2** (0.131 g, 0.204 mmol) and sodium triacetoxy borohydride (0.052 g, 0.249 mmol) were then added to the mixture and stirring was maintained for another 6 h. The reaction mixture was diluted with DCM (50 mL) and then washed with water (20 mL), citric acid (30 mL), NaHCO$_3$ (30 mL), brine (20 mL), dried over Na$_2$SO$_4$ and concentrated. Flash chromatography of the residue over alumina gel (50–90% EtOAc in hexanes) gave **3c** as a pale-yellow oil in 91% yield. ^{1}H NMR (600 MHz, CD$_2$Cl$_2$) δ 7.46–7.30 (m, 20H), 5.57 (s, 8H), 4.36 (t, $J = 7.5$ Hz, 8H), 3.57–3.55 (m, 4H), 3.52–3.51 (m, 4H), 3.45 (s, 12H), 2.88 (t, $J = 7.8$ Hz, 8H), 2.75 (t, $J = 7.2$ Hz, 4H), 1.74–1.69 (m, 4H), 1.54 (s, 36H), 1.32 (m, 4H), 1.31 (s, 72H); ^{13}C NMR (150 MHz, CD$_2$Cl$_2$) δ 166.1, 161.8, 161.6, 160.7, 155.9, 153.1, 149.8, 135.7, 129.0, 128.9, 128.9, 93.2, 84.0, 83.2, 71.0, 70.6, 70.4, 69.7, 51.7, 51.5, 41.9, 35.4, 28.5, 28.4, 28.3, 28.2, 28.1; HRMS (ESI+) calcd for C$_{134}$H$_{185}$N$_{26}$O$_{35}$ [M + H]$^+$ 2718.349; found 2718.349.

Synthesis of compound 4c. Compound **3c** (0.168 g, 0.062 mmol) was stirred in a solution of TFA (6 mL) and DCM (2 mL) for 72 h. Et$_2$O (60 mL) was then added and the white precipitate formed, was centrifuged down. The residual solid was resuspended in Et$_2$O, sonicated and centrifuged down. This process was repeated until spotting of the Et$_2$O produced no UV active spot. The white solid was dried under vacuum for 72 h to yield the desired compound **4c** as a white solid (C$_{46}$H$_{64}$N$_{26}$O$_{11}$ + 5.25 TFA + H$_2$O + 0.25 Et$_2$O, 99%).

^{1}H NMR (600 MHz, d1-TFA) δ 4.78–4.62 (m, 8H), 3.90–3.71 (m, 24H), 3.14 (d, $J = 7.8$ Hz, 12H), 2.18 (s, 4H); ^{13}C NMR (150 MHz, D$_2$O/d1-TFA) δ 163.39, 161.49, 157.45, 157.26, 150.63, 83.92, 71.05, 70.83, 69.03, 53.87, 52.49, 38.23, 28.77, 24.38; MALDI-TOF MS (THAP, positive mode) calcd for C$_{46}$H$_{65}$N$_{26}$O$_{11}$ [M + H]$^+$ 1157.5320; found 1157.5316; anal. calcd for C$_{46}$H$_{64}$N$_{26}$O$_{11}$(CF$_3$CO$_2$H)$_{5.25}$(H$_2$O)(C$_4$H$_{10}$O)$_{0.25}$, C, 38.53; H, 4.15; N, 20.32; found C, 38.63, H, 4.17, N, 20.39.

For self-assembly, an aliquot of the TFA salt of **4c** was converted to the HCl salt. Compound **4c** (TFA salt) (0.036 g, 0.020 mmol) was dissolved in 1 M hydrochloric acid (15 mL), followed by removal of water under reduced pressure. This process was repeated two more times before the solid was dried under vacuum for 72 h to give the HCl salt of **4c** as a white solid (C$_{46}$H$_{64}$N$_{26}$O$_{11}$ + 8 HCl + 2.5H$_2$O + 0.6 Et$_2$O, 62%). MALDI-TOF MS (HCCA, positive mode) calcd for C$_{46}$H$_{65}$N$_{26}$O$_{11}$ [M + H]$^+$ 1157.5320; found 1157.5307; anal. calcd for C$_{46}$H$_{64}$N$_{26}$O$_{11}$(HCl)$_8$(H$_2$O)$_{2.5}$(C$_4$H$_{10}$O)$_{0.6}$; C, 37.79; H, 5.44; N, 23.67, found C, 37.81, H, 5.47, N, 23.53.

Conclusions

We have designed a tetra-G∧C system, which has the ability to self-assemble into nanotubes of about 3 nm in diameter, by adopting a 4-fold stack. The rosette formation relied mainly on the 72 intermolecular hydrogen bonding and stacking of the intramolecular G∧C units. The relative stabilities of the different conformers were evaluated computationally. Despite the limited flexibility of the hydrophobic butyl linker in the strand, the negative association free energies of different conformations in water suggested that the solvent plays an important role in the formation of such superstructures. We anticipate that this quad-RNT system will allow the attachment of functional groups with higher steric bulk on the periphery of the nanotubes compared to the single or twin G∧C system and would be useful towards the design of advanced functionalized RNTs for cargo-carrying capabilities under physiological conditions in targeted applications.

Data availability

The data supporting this article are included as part of the ESI.†

Author contributions

The manuscript was written through contributions of all authors. All authors have given approval to the final version of the manuscript.

Conflicts of interest

The authors declare no competing financial interest.

Acknowledgements

References

1 A. Klug, *Angew Chem. Int. Ed. Engl.*, 1983, **22**, 565–582.

2 N. C. Seeman, *Trends Biotechnol.*, 1999, **17**, 437–443.

3 T. L. Schlick, Z. Ding, E. W. Kovacs and M. B. Francis, *J. Am. Chem. Soc.*, 2005, **127**, 3718–3723.

4 D. Ajami, J. L. Hou, T. J. Dale, E. Barrett and J. Rebek Jr, *Proc. Natl. Acad. Sci. U. S. A.*, 2009, **106**, 10430–10434.

5 A. M. Carmona-Ribeiro, *Chem. Soc. Rev.*, 2001, **30**, 241–247.

6 C. Schmuck, *Angew Chem. Int. Ed. Engl.*, 2007, **46**, 5830–5833.

7 C. F. van Nostrum, *Adv. Mater.*, 1996, **8**, 1027–1030.

8 N. P. Dharmarajan, D. Vidyasagar, J. H. Yang, S. N. Talapaneni, J. Lee, K. Ramadass, G. Singh, M. Fawaz, P. Kumar and A. Vinu, *Adv. Mater.*, 2024, **36**, e2306895.

9 F. B. Ilhami, Y. S. Birhan and C. C. Cheng, *ACS Biomater. Sci. Eng.*, 2024, **10**, 234–254.

10 S. Huang, H. Yu and Q. Li, *Adv. Sci.*, 2021, **8**, 2002132.

11 R. Chakrabarty, P. S. Mukherjee and P. J. Stang, *Chem. Rev.*, 2011, **111**, 6810–6918.

12 J.-M. Lehn, *Angew Chem. Int. Ed. Engl.*, 1990, **29**, 1304–1319.

13 F. J. Hoeben, P. Jonkheijm, E. W. Meijer and A. P. Schenning, *Chem. Rev.*, 2005, **105**, 1491–1546.

14 J. P. Mathias, J. A. Zerkowski, C. T. Seto, E. E. Simanek and G. M. Whitesides, *J. Am. Chem. Soc.*, 1994, **116**, 4316–4325.

15 S. Kabata Glowacki, K. Koszinowski, D. Hubner, H. Frauendorf, P. Vana and U. Diederichsen, *Chemistry*, 2020, **26**, 12145–12149.

16 D. T. Bong, T. D. Clark, J. R. Granja and M. R. Ghadiri, *Angew Chem. Int. Ed. Engl.*, 2001, **40**, 988–1011.

17 A. Marsh, M. Silvestri and J.-M. Lehn, *Chem. Commun.*, 1996, 1527–1528.

18 M. Mascal, N. M. Hext, R. Warmuth, M. H. Moore and J. P. Turkenburg, *Angew Chem. Int. Ed. Engl.*, 1996, **35**, 2204–2206.

19 H. Fenniri, P. Mathivanan, K. L. Vidale, D. M. Sherman, K. Hallenga, K. V. Wood and J. G. Stowell, *J. Am. Chem. Soc.*, 2001, **123**, 3854–3855.

20 H. Fenniri, B.-L. Deng and A. E. Ribbe, *J. Am. Chem. Soc.*, 2002, **124**, 11064–11072.

21 G. Borzsonyi, A. Alsbaiee, R. L. Beingessner and H. Fenniri, *J. Org. Chem.*, 2010, **75**, 7233–7239.

22 J. G. Moralez, J. Raez, T. Yamazaki, R. K. Motkuri, A. Kovalenko and H. Fenniri, *J. Am. Chem. Soc.*, 2005, **127**, 8307–8309.

23 U. D. Hemraz, M. El-Bakkari, T. Yamazaki, J.-Y. Cho, R. L. Beingessner and H. Fenniri, *Nanoscale*, 2014, **6**, 9421–9427.

24 A. L. Chun, J. G. Moralez, H. Fenniri and T. J. Webster, *Nanotechnology*, 2004, **15**, S234–S239.

25 L. Zhang, U. D. Hemraz, H. Fenniri and T. J. Webster, *J. Biomed. Mater. Res., Part A*, 2010, **95A**, 550–563.

26 A. Childs, U. D. Hemraz, N. J. Castro, H. Fenniri and L. G. Zhang, *Biomed. Mater.*, 2013, **8**, 065003.

27 L. Sun, L. Zhang, U. D. Hemraz, H. Fenniri and T. J. Webster, *Tissue Eng.*, 2012, **18**, 1741–1750.

28 L. Sun, D. Li, U. D. Hemraz, H. Fenniri and T. J. Webster, *J. Biomed. Mater. Res., Part A*, 2013, **102A**(10), 3446–3451.

29 L. Zhang, F. Rakotondradany, A. J. Myles, H. Fenniri and T. J. Webster, *Biomaterials*, 2009, **30**, 1309–1320.

30 X. Zhou, S. Tenaglio, T. Esworthy, S. Y. Hann, H. Cui, T. J. Webster, H. Fenniri and L. G. Zhang, *ACS Appl. Mater. Interfaces*, 2020, **12**, 33219–33228.

31 J.-Y. Cho, P. Bhowmik, P. L. Polowick, S. G. Dodard, M. El-Bakkari, G. Nowak, H. Fenniri and U. D. Hemraz, *ACS Omega*, 2020, **5**, 24422–24433.

32 T. Yamazaki and H. Fenniri, *J. Mol. Liq.*, 2016, **217**, 70–74.

33 U. Ho, M. El-Bakkari, A. Alshamsan, J. Y. Cho, T. Yamazaki, U. D. Hemraz and H. Fenniri, *Biomater. Sci.*, 2023, **11**, 7169–7178.

34 H. N. M. Ali and A. A. Gonzales 3rd, *Molecules*, 2023, **28**, 7853.

35 D. Roy and A. Kovalenko, *Thermo*, 2023, **3**, 375–395.

36 P. Tripathi, L. Shuai, H. Joshi, H. Yamazaki, W. H. Fowle, A. Aksimentiev, H. Fenniri and M. Wanunu, *J. Am. Chem. Soc.*, 2020, **142**, 1680–1685.

37 J. Raez, J. G. Moralez and H. Fenniri, *J. Am. Chem. Soc.*, 2004, **126**, 16298–16299.

38 B.-L. Deng, R. L. Beingessner, R. S. Johnson, N. K. Girdhar, C. Danumah, T. Yamazaki and H. Fenniri, *Macromolecules*, 2012, **45**, 7157–7162.

39 C. Igci, O. Karaman, Y. Fan, A. A. Gonzales, H. Fenniri and G. Gunbas, *Sci. Rep.*, 2018, **8**, 15949.